This CVPR paper is the Open Access version, provided by the Computer Vision Foundation.
Except for this watermark, it is identical to the accepted version;
the final published version of the proceedings is available on IEEE Xplore.

ManTra-Net: Manipulation Tracing Network For Detection And Localization of Image Forgeries With Anomalous Features

Yue Wu*§, Wael AbdAlmageed*, and Premkumar Natarajan*§
*USC Information Sciences Institute, Marina del Rey, CA, USA
§Amazon, Manhattan Beach, CA, USA
wuayue@amazon.com, {wamageed, pnataraj}@isi.edu

Abstract

To fight against real-life image forgery, which commonly involves different types and combined manipulations, we propose a unified deep neural architecture called ManTra-Net. Unlike many existing solutions, ManTra-Net is an end-to-end network that performs both detection and localization without extra preprocessing and postprocessing. ManTra-Net is a fully convolutional network and handles images of arbitrary sizes and many known forgery types such splicing, copy-move, removal, enhancement, and even unknown types. This paper has three salient contributions. We design a simple yet effective self-supervised learning task to learn robust image manipulation traces from classifying 385 image manipulation types. Further, we formulate the forgery localization problem as a local anomaly detection problem, design a Z-score feature to capture local anomaly, and propose a novel long short-term memory solution to assess local anomalies. Finally, we carefully conduct ablation experiments to systematically optimize the proposed network design. Our extensive experimental results demonstrate the generalizability, robustness and superiority of ManTra-Net, not only in single types of manipulations/forgeries, but also in their complicated combinations.

Figure 1. Win the Photoshop battle [27] using ManTra-Net, which is capable of localize various complicated real-life forgeries. Columns from left to right are: pristine donor image, forged image (also the input of ManTra-Net), and the ManTra-Net's prediction.

1. Introduction

Image forgery has recently become an epidemic, negatively affecting many aspects of our life, *e.g.*, fake news, Internet rumors, insurance fraud, blackmail, and even academic publications [51]. Yet, most cases of image forgeries are not detected. Just in biomedical research publications alone, *3.8% of 20,621 papers (published in 40 scientific journals from 1995 to 2004) contained problematic figures, with at least half exhibiting features suggestive of deliberate manipulation* [12]. In 2014, Stern et al. [41] estimate that *each of the retracted articles could account for a mean of $392,582 in direct costs*, implying much higher indirect costs caused by misled research—and this is only in the biomedical field and these numbers are five years outdated. It is therefore imperative to develop new algorithms to assist in the fight against image manipulation and forgery.

Many image forgery techniques exist. However, splicing [19, 44, 28], copy-move [18, 43, 37, 46, 45], removal [58], and enhancement [9, 10, 17] are the four that have been studied the most. Both splicing and copy-move involve pasting image content to the target (*i.e.*, forged)

This work was done prior to Amazon involvement of the authors.

image. However, in splicing the added content is obtained from a different image, while in copy-move it is from the target image. Removal, also known as inpainting, removes a selected image region (*e.g.* hiding an object) and fills the space with new pixel values estimated from background. Finally, image enhancement is a wide collection of local manipulations, such as sharpening, brightness adjustment, *etc*. Depending on the characteristics of the forgery, different clues can be used as the foundation for detection/localization. These clues include JPEG compression artifacts [25, 30, 5], edge inconsistencies [39, 53], noise pattern [33, 49, 20], color consistency [21], visual similarity [44, 45, 46], EXIF consistency [28], and camera model [14, 13]. However, real-life forgeries are more complex, as illustrated in Fig. 1, and malicious forgers often use a sequence of manipulations to hide the forgery, including up-to-date techniques such as deep neural network-based (DNN) face swapping [36, 57], as shown in Fig. 1-(c). This compels us to develop new unified forgery detection techniques that are not limited to one or several known manipulation types but capable of handling more complicated and/or unknown types.

Another issue that has often been overlooked is forgery region localization. Most of the existing methods [9, 25, 37, 38, 49] only focus on image-level detection—whether or not an image is forged. Furthermore, methods that provide localization capabilities often rely on heavy, time-consuming pre- and/or post-processing, *e.g.*, patch extraction [53], expectation-maximization [19, 20], feature clustering [14, 11, 32, 28], segmentation [32, 28, 15], *etc*. Finally, the disconnection between feature learning and forgery mask generation suggest an under-optimized forgery detection and localization method.

In this paper, we address the above issues, and propose a novel solution called ManTra-Net for generalized image forgery localization/detection (IFLD). It detects forged pixels by identifying local anomalous features, and thus is not limited to a specific forgery or manipulation type. It is an end-to-end solution, and thus no need to apply pre- and/or post-processing. It is also composed of all trainable modules, and thus all modules can be jointly optimized towards to the IFLD task. The remainder of this paper is organized as follows. Sec. 2 discusses the related works and gives the ManTra-Net overview. Sec. 3 presents our study to obtain robust image manipulation-trace features. Sec. 4 proposes our local anomaly detection network. Sec. 5 shows our experimental results; and we conclude this paper in Sec. 6.

2. Manipulation Tracing Network

2.1. Related Works

Table 1 summarizes the most notable image forgery detection and localization work in the last four years. Several

	Method	Clue/Feature	DNN Type	Localize?	PP?	Target Forgery
2015	[33]	Noise pattern	N/a	Patch-Lv	Y	splicing
	[18]	Patch co-occur.	N/a	Pixel-Lv	Y	copy-move
	[16]	Pixel residual	DNN	–	–	removal
	[21]	Color consistency	N/a	Patch-Lv	Y	splicing
2016	[9]	Artifacts	AlexNet	–	–	4
	[25]	DCT correlation	N/a	–	–	splicing
	[37]	Pixel residual	DNN	–	–	splicing, copy-move
2017	[5]	DCT Artifacts	DNN	N/a	N/a	1
	[17]	Artifacts	VGG	Patch-Lv	N	7
	[30]	DCT correlation	N/a	–	–	splicing
	[39]	Edge consistency	MulitTaskFCN	Pixel-Lv	N	splicing
	[44]	Similarity	VGG + FCN	Pixel-Lv	N	splicing
	[54]	Artifact	2Br-DNN	Patch-Lv	N	1
2018	[8]	DNN implicit	CNN	–	–	1
	[28]	EXIF-Consistency	SiameseNet	Pixel-Lv	Y	splicing
	[35]	Camera model	DNN	Patch-Lv	Y	splicing
	[42]	Pixel co-occurr.	CNN	–	–	1
	[46]	Patch co-occurr.	CNN	Pixel-Lv	N	copy-move
	[55]	Artifacts+Noise	FastRCNN	Region-Lv	N	splicing, copy-move, removal
	[58]	DNN implicit	FCN	Pixel-Lv	N	removal
	Ours	Anomalous feature	FCN	Pixel-Lv	N	splicing, copy-move, removal, K

Table 1. Summary of recent IFLD methods. Non-DNN methods are labeled as N/a. Detection only methods are labeled as –. PP stands for pre-/post-processing, and target forgery types are color coded as follows: splicing, copy-move, removal, and K-type enhancement.

trends can be observed — (1) varieties of clue/feature are used, ranging from handcrafted features, such as DCT correlation to completely implicit learned DNN features, (2) even though DNN methods are becoming more popular, no dominant DNN architecture, or more precisely, almost not any two DNN approaches, adopt the same network architecture, and (3) most methods focus on one specific type of forgery. A more comprehensive review can be found in [6].

2.2. Overview

As shown in Fig. 2, the proposed ManTra-Net solution is composed of two sub-networks, *i.e.*, the image manipulation-trace feature extractor that creates a unified feature representation, and the local anomaly detection network (LADN) for directly localizing forgery regions without postprocessing. We make three major contributions to the IFLD community.

First, we reinvent the image manipulation trace feature, which was limited to differentiate a small number of known manipulations [17, 5], but is now capable to distinguish 385 types of known manipulations, and is robust to encode manipulations of unknown types, even for those DNN-based manipulations (*e.g.* deep image inpainting) and sequential manipulations (*e.g.* enhancement, resizing, and compression in a row.) We demonstrate that this feature is suitable to IFLD tasks and that it can be effectively and efficiently learned from the self-supervised learning task – image manipulation classification (IMC).

Second, we abandon the common semantic segmenta-

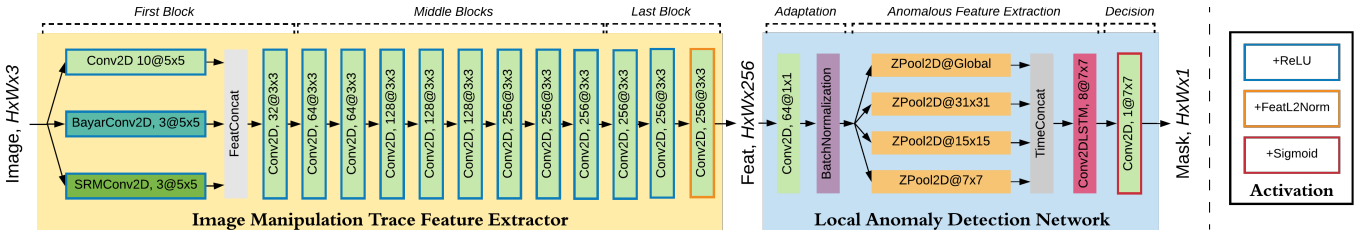

Figure 2. The overview of the proposed ManTra-Net architecture for the image forgery localization and detection task. Detailed discussions of the two sub-nets, *i.e.* image manipulation tracing feature extractor and local anomaly detection network, can be found in Sec. 3 and Sec. 4, respectively. A layer is color framed if additional non-linear activation is applied.

tion like IFLD formulations [58, 56, 39], but formulate the IFLD task as a local anomaly detection problem to improve the model generalizability. More precisely, we want to learn a decision function mapping from the difference between a local feature and its reference to its forgery label. To fulfill this goal, we invent a simple yet effective LADN architecture that mimics the human decision process by using two novel designs: (1) `ZPool2D` DNN layer, which standardizes the difference between a local feature and its reference in the Z-score manner; and (2) the far-to-near analysis, which performs the `Conv2DLSTM` sequential analysis on `ZPool2D` feature maps pooled from different resolutions.

Finally, we carefully conduct ablation experiments to systematically optimize both the IMC and LADN architectures, and provide theoretical groundings and/or experimental results to support our network designs.

2.3. Experimental Setup

To systematically study manipulation trace feature and anomaly detection, we use the following common setup for all ablation experiments, unless otherwise specified.

For manipulation trace feature, we use the *Dresden Image Database* [24] for pristine base images. Training, validation, and testing are divided with respect to image IDs with the ratio of 8:1:1. Each image is further broken into 256×256 patches. After rejecting patches with high homogeneity (*i.e.*, intensity deviation < 32), we have 1.25M patches in total. We synthesize a sample for image manipulation classification by: (1) selecting a random patch P and a random manipulation $y(\cdot)$, both in a uniform random manner, (2) applying manipulation y to P, and 3) cropping a random 128×128 region in $y(P)$ as X. This (X, y) pair is a sample of input and output for the classification task.

The *Kaggle Camera Model Identification* (KCMI) dataset [4] is used to check the generalizability and sensitivity of a manipulation classification network. It contains 10 camera models with 2475 samples. To evaluate KCMI performance, we randomly divide the dataset into two halves—one half to fit a (K=7) nearest-neighbor classifier, and the other half to test. The camera model feature is obtained by averaging over all manipulation trace features in the center 512×512 patch of a given image.

For anomaly detection, we use four synthetic datasets for training and validation — namely the splicing dataset from [44], the copy-move dataset from [45], the removal dataset synthesized by using built-in OpenCV inpainting function (with Dresden base images), and the enhancement dataset synthesized by using manipulation classification settings discussed previously. More precisely, we synthesize an enhanced sample by (1) introducing a random structured binary mask M (see [31]), (2) composing a forged image by using $Z = P \cdot (1-M) + y(P) \cdot M$, where P and $y(\cdot)$ are a pristine patch and a random manipulation, respectively. The resulting (Z, M) pair is a sample of input and output for an LADN task. Training patch size is set to 256×256.

In terms of training settings, we set batch size to 64 and 1000 batches per epoch, and use the `Adam` optimizer with the initial learning rate of 1e-4 but without decay. This learning rate will be halved if validation loss fails to improve for 20 epochs. The image manipulation classification and anomaly detection tasks are optimized towards the `cross-entropy` loss.

3. Manipulation-Trace Feature

In this section, we study the image manipulation trace feature extractor (see the yellow shaded block in Fig. 2) via the image manipulation classification problem. Although image manipulation trace feature have been previously used for forgery detection and localization purposes for a long time, the total number of image manipulations was usually below 10 — *e.g.*, [17, 5] use 7 and 9 types, respectively. Such few types of manipulations is clearly inadequate for a unified feature representation. We therefore systematically study manipulations with more types and finer differences, with 385 manipulation types. To the best of our knowledge, we this work is the first to consider this large number of fine-grained manipulation types.

3.1. Study of Backbone Network Architecture

Since no dominant IFLD network architecture (see Table 1) and very few studies on IMC networks, we conduct backbone architecture comparisons among three

networks—VGG [40], ResNet [26], and DnCNN [52], all of which are proposed outside of the IFLD community but used previously for IFLD [20, 28, 44, 45, 55].

For fair comparison, we customize backbone models to have the same receptive field sizes, and similar numbers of filters and hyper-parameters (see Table 2). It is worth noting that all listed manipulation classification models are fully convolutional networks (FCN) (*i.e.* no down-sampling or `Dense` layer).

	IMC-VGG	IMC-ResNet	IMC-DnCNN
FirstBlock	[16@(3,3) ReLU]×2	[16@(3,3) ReLU]×1	[72@(3,3) ReLU]×1
MiddleBlock	[16k@(3,3) ReLU]×m	[16(k−1)@(3,3) ReLU, 16(k−1)@(3,3) BN + ReLU, ProjShortcut]×m	[72@(3,3) BN + ReLU]×m
m	[2, 3, 2]	[1, 1, 1, 1]	[1,1,1,1,1,1,1,1,1]
LastBlock	[128@(3,3) + L2Norm]×1		
DecisionBlock	[7@(3,3) + Softmax]×1		
#Conv2D	11	14	12
#Param.	487K	465K	482K
IMC-7 Train Acc.	94.5%	94.3%	94.7%
IMC-7 Valid Acc.	92.1%	90.8%	91.2%
KCMI Test Acc	55.1%	48.1%	49.4%

Table 2. IMC-7 network architecture and performance comparisons. Building blocks are shown in brackets. N@(3,3) indicates a `Conv2D` layer with N filters of kernel size 3-by-3. k in IMC-VGG is the block index, *e.g.* the number of filters used in block 2 is $32 = 16 \times 2$. m is the unit repetitiveness; *e.g.* $m = [2, 3, 2]$ indicates three middle blocks repeat the unit 2, 3, and 2 times, respectively. `Conv2D` of projection shortcut in ResNet is not listed.

To speed up training and offer training to many models, we study the simple IMC-7 problem, *i.e.*, classification on the seven general manipulation families: *compression, blurring, morphology, contrast manipulation, additive noise, resampling, and quantization*. Specifically, we train each architecture with three models, but only the model with the best validation loss is reported in the lower half of Table 2. It turns out that all three architectures achieve similar IMC-7 performance. However, VGG outperforms the rest with a smaller gap between training and validation, but a much higher accuracy in KCMI testing. We thus use the VGG architecture in the remainder of our studies.

1st Conv. Layer	`Conv2D`	`Conv2D`	`BayarConv2D`	`SRMConv2D`	Combined
#Filters	16	16	3	3	10+3+3
Kernel Size	(3,3)	(5,5)	(5,5)	(5,5)	(5,5)
IMC-7 Train Acc.	94.5%	94.9%	93.8%	95.2%	95.5%
IMC-7 Valid Acc.	92.1%	92.5%	92.0%	93.1%	93.4%
KCMI Test Acc.	55.1%	55.2%	49.9%	57.1%	57.2%

Table 3. IMC-7 performance comparisons on feature type.

We also study the feature choice of the first layer. We compare the known optimal settings for `SRMConv2D` from [55] and `BayarConv2D` from [10] with the classic `Conv2D` layers, and a combined version of all three, which is simply the feature concatenation as shown in Fig. 2. From Table 3, it is safe to conclude that different feature types make small differences in IMC-7 performance, usually 1% to 2%, while using the combined setting gives the best performance. We therefore use the combined features for the first convolutional layer.

3.2. Study of Fine-Grained Manipulation Types

To make the manipulation trace feature more sensitive and robust, we study the IMC problem for more and finer manipulation types. Specifically, we gradually break down the seven manipulation families (hierarchy level 0) until they are individual algorithms (hierarchy level 5). For example, the *blurring* family is broken down to *Gaussian blurring*, *box blurring*, *wavelet denoising*, and *median filtering* for hierarchy level 1. Then we proceed to an even finer level by specifying algorithm parameters, *e.g.*, *Gaussian blurring* w.r.t. small kernel sizes like 3, 5, and 7 for hierarchy level 2. This continues on until reaching the individual kernel size for hierarchy level 5. The complete hierarchy map is included in our code repository, as there are different hierarchy levels for 7, 25, 49, 96, 185, and 385 classes for manipulation classification.

All IMC models in this study share the same VGG network architecture discussed earlier, except for the number of output classes in the decision block (see Table 2). Their scores are listed in Table 4. Because of the predefined hierarchy map, an IMC trained on hierarchy i can be used to also predict labels of hierarchy j for $i > j$. All underlined scores in Table 4 are obtained in this way. It is clear that fine-grained manipulation classes help improve, not only validation accuracy for lower hierarchies, but also the KCMI accuracy from 57.2% to 82.6%.

Hierarchy Level	HL0	HL1	HL2	HL3	HL4	HL5
# IMC Classes	7	25	49	96	185	385
IMC-7 Valid. Acc.	93.4%	95.1%	96.1%	96.3%	96.3%	96.2%
IMC-25 Valid. Acc.	-	85.1%	85.7%	85.4%	85.5%	85.7%
IMC-49 Valid. Acc.	-	-	77.5%	79.6%	78.9%	79.2%
IMC-96 Valid. Acc.	-	-	-	72.4%	72.7%	73.2%
IMC-185 Valid. Acc.	-	-	-	-	53.4%	63.3%
IMC-385 Valid. Acc.	-	-	-	-	-	47.3%
KCMI Test Acc.	57.2%	62.7%	71.9%	78.4%	82.0%	82.6%

Table 4. IMC performance analysis w.r.t. manipulation types.

IMC-385 validation accuracy (47.3%) is relatively low. We therefore adjust the baseline IMC-VGG architecture in two orthogonal directions—(1) make it wider [50], *i.e.*, using more filters in each convolutional layer, and (2) make it deeper, *i.e.*, using more convolutional blocks. Both attempts improve the baseline performance, and the combination of wider and deeper (W&D) improves even more. Table 5 shows these results. We therefore use the IMC-VGG W&D architecture excluding the decision block for the manipulation trace feature extractor (see Fig. 2).

3.3. Discussions

The IMC performance can be further improved if a larger receptive field size is used. We, however, stop exploration

IMC-VGG	Baseline	Wider(W)	Deeper(D)	W&D
FirstBlock	$\begin{bmatrix}16@(3,3)\\ \texttt{ReLU}\end{bmatrix}\times 2$	$\begin{bmatrix}32@(3,3)\\ \texttt{ReLU}\end{bmatrix}\times 2$	$\begin{bmatrix}16@(3,3)\\ \texttt{ReLU}\end{bmatrix}\times 2$	$\begin{bmatrix}16@(3,3)\\ \texttt{ReLU}\end{bmatrix}\times 2$
MiddleBlock	$\begin{bmatrix}16k@(3,3)\\ \texttt{ReLU}\end{bmatrix}\times m$	$\begin{bmatrix}32k@(3,3)\\ \texttt{ReLU}\end{bmatrix}\times m$	$\begin{bmatrix}16k@(3,3)\\ \texttt{ReLU}\end{bmatrix}\times m$	$\begin{bmatrix}32k@(3,3)\\ \texttt{ReLU}\end{bmatrix}\times m$
m	[2, 3, 2]	[2, 3, 2]	[2, 3, 3]	[2, 3, 3]
LastBlock	$\begin{bmatrix}128@(3,3)\\ \texttt{L2Norm}\end{bmatrix}\times 1$	$\begin{bmatrix}256@(3,3)\\ \texttt{L2Norm}\end{bmatrix}\times 1$	$\begin{bmatrix}256@(3,3)\\ \texttt{ReLU}\\ 256@(3,3)\\ \texttt{L2Norm}\end{bmatrix}\begin{matrix}\times 2\\ \times 1\end{matrix}$	$\begin{bmatrix}256@(3,3)\\ \texttt{ReLU}\\ 256@(3,3)\\ \texttt{L2Norm}\end{bmatrix}\begin{matrix}\times 2\\ \times 1\end{matrix}$
DecisionBlock	$\begin{bmatrix}385@(3,3)+\texttt{Softmax}\end{bmatrix}$			
#Conv2D	11	11	14	14
#Receptive Filed	23 × 23	23 × 23	29 × 29	29 × 29
IMC-385 Top-1	47.3%	48.6%	45.7%	51.8%
IMC-385 Top-3	66.5%	69.9%	69.8%	72.0%
IMC-385 Top-5	75.3%	79.5%	79.4%	81.1%
IMC-385 Top-10	85.8%	90.7%	92.5%	93.1%
KCMI Test Acc	82.6%	83.1%	83.0%	83.6%

Table 5. IMC-385 performance comparisons using different architectures. Building blocks are shown in brackets. N@(3,3) indicates a `Conv2D` layer with N filters of kernel size 3-by-3.

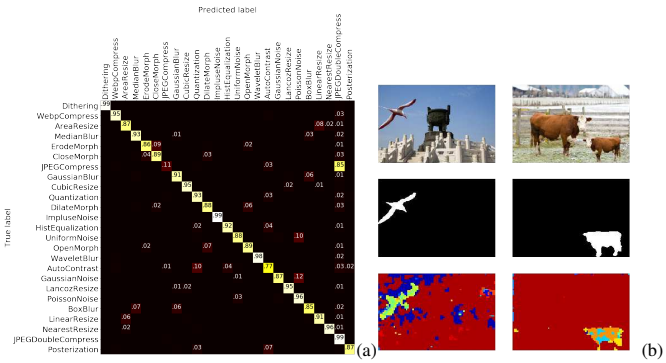

(a) (b)

Figure 3. IMC discussion items. (a) IMC-385 HL1 confusion matrix. (b) Sample IMC results, from top to bottom: testing image, ground truth forgery mask, and the IMC membership map (color coded in terms of HL1). Best viewed in color and zoom-in.

and stick to the IMC-VGG-W&D architecture to ensure the feature sensitivity to small manipulated regions.

Regarding the IMC-385 performance, Fig. 3-(a) illustrates the IMC-VGG-W&D confusion matrix at the hierarchy level 1 (with 25 classes). It is quite close to the identity matrix, and thus the most IMC-385 errors happen within the same type of manipulations, but with different parameters. Indeed, the only salient error in the confusion matrix is to misclassify `JPEGCompression` to `JPEGDoubleCompression`, possibly because most *pristine* images in the *Dresden* dataset are of the JPEG format, indicating that they are already compressed.

Though the KCMI testing results confirm the generalizability of the learned manipulation trace feature, we double check feature effectiveness for the IFLD task. As shown in Fig. 3-(b), one can easily identify the correspondences between the IMC membership maps and the ground truth forgery masks, indicating (1) the proposed IMC feature is useful for the IFLD task; and (2) one can easily identify forged regions by identify anomalous local features that are different from those in their surroundings.

4. Local Anomaly Detection Network

In this section, we propose a novel deep anomaly detection network architecture. As shown in Fig. 2, it is composed of three stages: (1) adaptation, which adapts the manipulation trace feature for the anomaly detection task; (2) anomalous feature extraction, which is inspired by human thinking and extracts anomalous features; and (3) decision, which holistically consider anomalous features and classify whether a pixel is forged or not. Since both adaptation and decision stages are straight-forward, we focus on the discussion of anomalous feature extraction.

4.1. Anomalous Feature Extraction

Given a feature map (*e.g.* the bottom row in Fig. 3-(b)), how a human identifies potential forged regions. Though this question can be answered differently, one can first identify the dominant feature of an image, and any feature sufficiently different from this dominant feature is thus anomalous. In the rest of section, we follow this intuition and discuss the solutions to the two key tasks (1) what is a dominant feature, and how to compute it, and (2) how to quantify the difference between a local feature and a reference dominant feature, and what is the best way in practice.

Let us start with simple solutions. One choice for the dominant feature is the average feature defined in Eq. (1)

$$\mu_F = \sum_{i=1}^{H}\sum_{j=1}^{W} F[i,j]/(HW) \tag{1}$$

where F is a raw feature tensor of size $H \times W \times L$. Similarly, one may use the raw difference in Eq. (2) to quantify the difference between a local feature and its reference.

$$D_F[i,j] = F[i,j] - \mu_F \tag{2}$$

Considering the generalizability, the normalized Z-score defined in Eq. (3) works better, (see Table 6)

$$Z_F[i,j] = D_F[i,j]/\sigma_F \tag{3}$$

where σ_F is the standard deviation of F as shown in Eq (4).

$$\sigma_F^2 = \sum_{i=1}^{H}\sum_{j=1}^{W} F[i,j]^2/(HW) - \mu_F^2 \tag{4}$$

In practice, we replace σ_F with σ_F^* as shown in Eq. (5)

$$\sigma_F^* = \text{maximum}(\sigma_F, \epsilon + w_\sigma), \tag{5}$$

where ϵ =1e-5 and w_σ is a learnable non-negative weight vector of the same length as σ_F.

To this end, feature Z_F encodes how different each local feature is from a reference feature, but Z_F suffers one major drawback when two more regions are manipulated differently. Say an image contains two disjoint forged regions

R_1 and R_2, while the rest is pristine background region B. Depending on the relative relationship among μ_{R_1}, μ_{R_2} and μ_B, feature μ_F may fail to represent the dominant μ_B. To simplify discussion, let F's feature dimension be 1. When $\mu_{R_1} \gg \mu_{R_2} > \mu_B$, μ_F can be some value much closer to μ_{R_2} than μ_B, implying Z_F is incapable of capture the anomalous region R_2.

One quick remedy is to compute the reference feature from a local but big enough window, which mitigates if not excludes the influence of features from other forged regions. Specifically, we compute the window-wise deviation feature,

$$D_F^{n\times n}[i,j] = F[i,j] - \mu_F^{n\times n}[i,j] \tag{6}$$

where $\mu_F^{n\times n}[i,j]$ is the average feature computed within the $n \times n$ window centered at (i,j) location through the standard `AveragePool2D` layer. However, we have no idea what n should be for a testing sample. We therefore follow the common multi-resolution analysis (*e.g.* [47]), and collect a series of Z-score features w.r.t. different window sizes n_1 through n_k as shown in Eq. (7).

$$Z_F^* = [Z_F^{n_1\times n_1}, \cdots, Z_F^{n_k\times n_k}, Z_F] \tag{7}$$

The process of converting from input feature F to a Z-score feature is referred as to `ZPool2D` in Fig. 2.

Although one can concatenate Z_F^* along the feature dimension and produce a 3D feature (size of $H\times W\times(k+1)L$) to represent the difference feature, this fails to capture the essence of human decision progress – the far-to-near analysis, *i.e.* one will move closer if he can't see something clearly. We, therefore, concatenate Z_F^* along the new artificial time dimension and produce a 4D feature of size $(k+1)\times H\times W\times L$. By using the `ConvLSTM2D` layer [48], the proposed anomaly detection network analyzes the Z-score deviation belonging to different window sizes in a sequential order. In other words, we look into a fine-grained Z-score map if we are uncertain, and thus conceptually follows the far-to-near analysis.

4.2. Anomaly Detection Ablation Experiment

We conduct a set of ablation experiments to study the performance of previously mentioned anomalous features using the ManTra-Net solution shown in Fig. 2. To ensure fair comparisons, all experiments (1) differ from each other only in the used anomaly detection feature; (2) share the same pretrained manipulation trace feature extractor; and (3) the manipulation trace feature extractor is set to non-trainable. One may refer to Sec. 2.3 for other settings.

Table 6 compares all features in terms of validation F_1 scores. It is clear that the Z-score difference is better, and that the more window sizes we consider, the better the overall performance is. For the sake of efficiency, we stop analyzing more windows. Compared to the feature-axis-concatenation (FAC), using the time-axis-concatenate (TAC) for Z_F^* feature further boosts performance by roughly 7% in absolute and 15% in relative.

Anomaly Detection Feature	Dataset Validation F1-Score				
	Splicing	CopyMove	Removal	Enhance	Overall
D_F	13.26%	2.33%	6.79%	36.07%	14.61%
Z_F	18.71%	5.01%	39.67%	72.45%	33.81%
FAC($[Z_F^{7\times7}, Z_F]$)	21.99%	9.20%	38.55%	74.59%	36.08%
FAC($[Z_F^{7\times7}, Z_F^{15\times15}, Z_F]$)	24.51%	11.47%	43.96%	75.78%	38.93%
FAC($[Z_F^{7\times7}, Z_F^{15\times15}, Z_F^{31\times31}, Z_F]$)	26.40%	17.88%	45.53%	77.92%	41.93%
TAC($[Z_F^{7\times7}, Z_F^{15\times15}, Z_F^{31\times31}, Z_F]$)	**38.58%**	**21.19%**	**52.32%**	**81.47%**	**48.39%**

Table 6. Anomaly detection features comparisons.

5. Experimental Evaluation

We have previously demonstrated the effectiveness of the used image manipulation-trace feature and the local anomaly detection network. In this section, we focus on evaluating the performance of the end-to-end ManTra-Net w.r.t. generalizability, sensitivity, robustness to postprocessing, and standard benchmarks.

Regarding evaluation metrics, we use the pixel-level area under the receiver operating characteristic curve (AUC) unless otherwise specified. It is important to note that due to the nature of local anomaly detection, ManTra-Net will label pristine pixels as forged if they are minorities. However, this behavior should not be penalized. We thus negate a ManTra-Net predicted mask when more than 50% of pixels are forged in ground truth, as suggested in [28].

5.1. Pre-trained Models and Generalizability Test

We train ManTra-Net models in the end-to-end manner using the four synthetic datasets mentioned in Sec. 2.3. The pretrained ManTra-Net models are available at [1].

To evaluate the generalizability of these models, the latest partial convolution-based CNN inpainting method [31] is selected as one typical out-of-domain DNN-based manipulation. In addition, the PhotoShop-battle dataset [27] is also used, because it is large (total 102,028 samples) and diverse (contributed from 31,272 online artists), and it reflects the level of real-life image manipulation. Since it only provides the image-level annotation (*i.e.*, pristine or forged) instead of the pixel-level, we evaluate model performance on this dataset by computing the image-level AUC, where the likelihood that an image is manipulated is simply computed as the average likelihood of all pixels.

As one can see in Table 7, the fully random model trained with full random weights does not generalize well because it overfits to the synthesized data, while the forgery clues presented in the used synthesized dataset are very different from those in the real world. The half freeze model trained by freezing the image manipulation-trace features (IMTF) and with random LADN weights does prevents

[1] https://github.com/ISICV/ManTraNet.git

overfitting, but eliminates the hope of finding better features for other forgery types, because the manipulation-trace feature is known to be optimized to the enhancement dataset (see the *Enhance* column in Table 6), but not to splicing, copy-move or removal. In contrast, the half random model that allows these weights to be updated at a lower learning rate of 5e-5 prevents overfitting and converges to a better feature representation for all forgery types. We thus use the ManTra-Net half random model in later experiments.

Name	IMTF Setting	Testing F1	[31] F1	[27]AUC
Fully Random (FR)	Random initialization	71.21%	68.37%	61.85%
Half Freeze (HF)	Freezed IMC-385	48.39%	72.54%	70.33%
Half Random (HR)	IMC-385 initialization	68.61%	78.32%	75.88%

Table 7. ManTra-Net performance under different settings.

5.2. Sensitivity and Robustness Evaluation

To evaluate how accurate ManTra-Net is to manipulations of different distortions, we conduct the following sensitivity study: (1) we synthesize manipulated samples using a manipulation function f and a method parameter p for 5,000 patches in the Dresden testing split; (2) we evaluate ManTra-Net on this synthesized dataset; and 3) we report its performance as one data point in Fig. 4. As shown in Fig. 4-(a), ManTra-Net is very accurate to additive noise and blurring methods, even for subtle manipulations like 3×3 `GaussianBlur`, while less accurate to compression methods, especially when the quality factor is above 95.

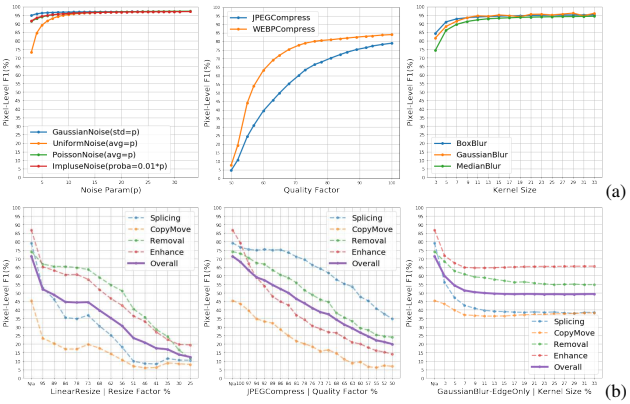

Figure 4. ManTra-Net's (a) sensitivity and (b) robustness tests.

In real life, one may disguise a forged image X with additional post-processing. Here we considered the three common postprocessing methods: (1) resizing X to a smaller size, (2) compressing X with a lower quality factor, and 3) smoothing X around the edges of forged regions. Instead of a raw testing sample from the four synthesized datasets, we feed in the pretrained ManTra-Net with the post-processed version, and compute the testing performance decay. These results are shown in Fig. 4-(b). ManTra-Net's overall performance almost drops linearly for `LinearResize` and `JPEGCompress`, which is much slower than the quadratic pixel reducing rate in resizing. Finally, though local blurring is known to be very effective in fooling edge-based forgery detection methods, ManTra-Net is quite immune to this type of attack.

5.3. Comparison Against SOTA Methods

Following [55], we compare ManTra-Net's performance against numbers reported in [55], which provides scores of the classic unsupervised methods: ELA [29], NOI1 [34], CFA1 [22], and the latest DNN-based solutions, MFCN [39] and J-LSTM [7] on the four benchmark datasets, namely NIST 2016 [3], CASIA [2], COVERAGE [43], and Columbia dataset [1]. These four datasets contain 564, 6044, 100, and 180 samples, respectively. It worth noting that we (1) use a pretrained model instead of a finetuned one, and (2) evaluate performance on the full dataset instead of a small testing split.

Methods	NIST		Columbia		COVERAGE		CASIA	
Forgery Types								
ELA [29]	0%	42.9%	0%	58.1%	0%	58.3%	0%	61.3%
EOI1 [34]	0%	48.7%	0%	54.6%	0%	58.7%	0%	61.2%
CFA1 [22]	0%	50.1%	0%	72.0%	0%	48.5%	0%	52.2%
J-LSTM [7]	72%	76.4%		N/a	75%	61.4%		N/a
RGB-N [55]	72%	93.7%	0%	85.8%	75%	81.7%	85%	79.5%
ManTra-Net	0%	79.5%	0%	82.4%	0%	81.9%	0%	81.7%

Table 8. (training%, AUC) performance comparisons. Highest scores and training% are highlighted in blue and red, respectively. Forgery types are color coded as: splicing, copy-move, removal, and enhancement.

These results are listed in Table 8. We rank second-place in the NIST and Columbia datasets. A big performance gap between ManTra-Net and that of the RGB-N method is found in the NIST dataset, possibly because this dataset contains many samples forged from the exact same or very similar base images—where finetuning could definitely help. On the Columbia dataset, we fall just slightly behind the best method RGB-N by 3%, since we do not rely on any specific clue. The RGB-N method explicitly analyzes the noise pattern, which is known to be super effective to the Columbia dataset [55].

On the COVERAGE and CASIA datasets, however, we achieve even better performance on a larger evaluation portion than the J-LSTM and RGB-N methods, which both apply dataset finetuning. One possible explanation why we performed better is that images in these dataset are much smaller than those in NIST and Columbia (*e.g.*, a typical CASIA image is of size 256×384, while it is common to see images larger than 1000×1000 in NIST), and are closer to the image size we used in training, which is 256×256.

It is safe to conclude that ManTra-Net: (1) clearly outperforms those classic unsupervised methods by a large margin, and (2) is comparable to those state-of-the-art DNN methods, even though we do not apply any model finetuning or post-processing. Importantly, one especially note-

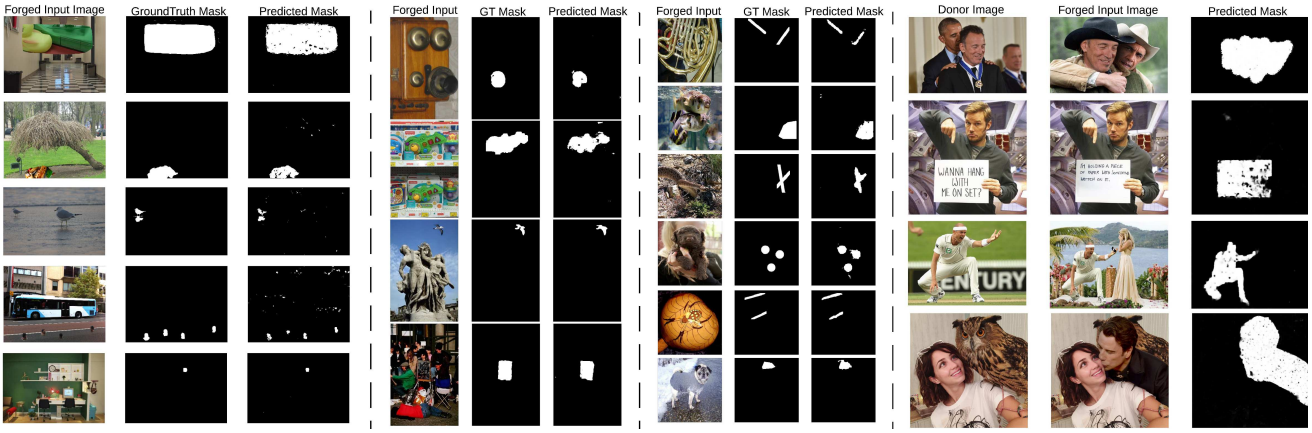

Figure 5. Sample ManTra-Net results. Mega columns are separated by dashed vertical lines. From left to right: the first two mega columns are results from NIST, Columbia, COVERAGE, and CASIA datasets; the third mega column are those forged by the deep inpainting technique [31]; and the last mega column are samples from the PS-battle dataset. Additional PS-battle results can be found in Fig. 1. ManTra-Net is capable to work in the real-life scenario, including but not limited (1) multiple forgery regions, (2) small manipulations, (3) compound manipulations, and (4) arbitrary input image sizes.

worthy feature is that the proposed ManTra-Net achieves very consistent performance across all testing datasets, indicating that it does generalize well on different datasets. Qualitative results can be found in Fig. 5. In terms of processing speed, ManTra-Net takes roughly 0.8 seconds per image (1024×768) on a single NVIDIA 1080Ti GPU.

5.4. Limitations

Detection of real-life image forgery is a difficult problem. We observed that ManTra-Net may fail when: (1) a forged image is fully regenerated (*e.g.* using the style transfer [23]), see Fig. 6-(a); (2) a forged image is intentionally contaminated with highly correlated noise, see Fig. 6-(b); and (3) multiple regions are manipulated differently, see Fig. 6-(c). As shown in Fig. 6-(c), both the text region and the wombat region are manipulated. ManTra-Net finds the text region but not the wombat region. We find that a quick remedy is to ask a user to select a region of interest before applying ManTra-Net, and this time we successfully catch the wombat. This indicates that ManTra-Net can be a computer-aid IFLD tool for humans.

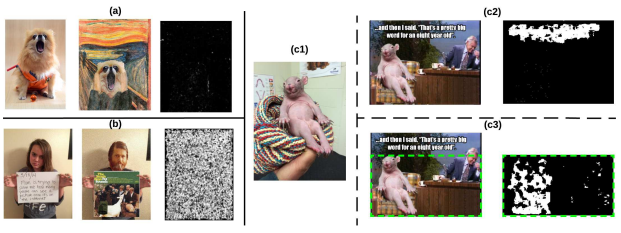

Figure 6. Failure cases. (a), (b), and (c) are results of the PS-battle samples cr3n0xh_0,cg869bx_0, and cjulwwp_0. Three images in each set of result is arranged as donor image, forged image, and predicted mask. Zoom-in for more details.

6. Conclusion

In this paper, we introduce a novel end-to-end DNN solution to image forgery localization called ManTra-Net. It first extracts image manipulation trace features for a testing image, and identifies anomalous regions by assessing how different a local feature is from its reference features. Our extensive experimental results using only pretrained models demonstrate that the proposed ManTra-Net is sensitive to subtle manipulations, and robust to postprocessing disguising manipulations, and that it attains good generalizability to unseen data and unknown manipulation types, even for those latest DNN-based manipulations like face swapping [36] and deep image inpainting [32]. One may further improve the ManTra-Net performance or adapt it to new forgery types by simply introducing more manipulation types to the IMC task and/or adding more training samples to the end-to-end IFLD task.

Acknowledgement

This work is based on research sponsored by the Defense Advanced Research Projects Agency under agreement number FA8750-16-2-0204. The U.S. Government is authorized to reproduce and distribute reprints for governmental purposes notwithstanding any copyright notation thereon. The views and conclusions contained herein are those of the authors and should not be interpreted as necessarily representing the official policies or endorsements, either expressed or implied, of the Defense Advanced Research Projects Agency or the U.S. Government.

References

[1] Image splicing detection evaluation dataset, 2004. http://www.ee.columbia.edu/ln/dvmm/downloads/AuthSplicedDataSet/AuthSplicedDataSet.htm.

[2] CASIA tampered image detection evaluation dataset, 2012. forensics.idealtest.org/casiav2.

[3] NIST manipulation evaluation dataset, 2016. https://www.nist.gov/itl/iad/mig/nimble-challenge-2017-evaluation.

[4] IEEE's signal processing society - camera model identification, 2018. https://www.kaggle.com/c/sp-society-camera-model-identification.

[5] I. Amerini, T. Uricchio, L. Ballan, and R. Caldelli. Localization of jpeg double compression through multi-domain convolutional neural networks. In *IEEE Conference on Computer Vision and Pattern Recognition Workshops*, volume 3, 2017.

[6] K. Asghar, Z. Habib, and M. Hussain. Copy-move and splicing image forgery detection and localization techniques: a review. *Australian Journal of Forensic Sciences*, 49(3):281–307, 2017.

[7] J. H. Bappy, A. K. Roy-Chowdhury, J. Bunk, L. Nataraj, and B. Manjunath. Exploiting spatial structure for localizing manipulated image regions. In *IEEE International Conference on Computer Vision*, pages 4970–4979, 2017.

[8] M. Barni, A. Costanzo, E. Nowroozi, and B. Tondi. Cnn-based detection of generic contrast adjustment with jpeg post-processing. In *IEEE International Conference on Image Processing*, pages 3803–3807. IEEE, 2018.

[9] B. Bayar and M. C. Stamm. A deep learning approach to universal image manipulation detection using a new convolutional layer. In *ACM Workshop on Information Hiding and Multimedia Security*, pages 5–10. ACM, 2016.

[10] B. Bayar and M. C. Stamm. Constrained convolutional neural networks: A new approach towards general purpose image manipulation detection. *IEEE Transactions on Information Forensics and Security*, 13(11):2691–2706, Nov 2018.

[11] G. Bhartiya and A. S. Jalal. Forgery detection using feature-clustering in recompressed JPEG images. *Multimedia Tools and Applications*, 76(20):20799–20814, 2017.

[12] E. M. Bik, A. Casadevall, and F. C. Fang. The prevalence of inappropriate image duplication in biomedical research publications. *MBio*, 7(3):e00809–16, 2016.

[13] L. Bondi, L. Baroffio, D. Güera, P. Bestagini, E. J. Delp, and S. Tubaro. First steps toward camera model identification with convolutional neural networks. *IEEE Signal Processing Letters*, 24(3):259–263, 2017.

[14] L. Bondi, S. Lameri, D. Güera, P. Bestagini, E. J. Delp, and S. Tubaro. Tampering detection and localization through clustering of camera-based CNN features. In *IEEE Conference on Computer Vision and Pattern Recognition Workshops*, pages 1855–1864, 2017.

[15] C. Chen, S. McCloskey, and J. Yu. Image splicing detection via camera response function analysis. In *IEEE Conference on Computer Vision and Pattern Recognition*, pages 5087–5096, 2017.

[16] J. Chen, X. Kang, Y. Liu, and Z. J. Wang. Median filtering forensics based on convolutional neural networks. *IEEE Signal Processing Letters*, 22(11):1849–1853, 2015.

[17] H.-Y. Choi, H.-U. Jang, D. Kim, J. Son, S.-M. Mun, S. Choi, and H.-K. Lee. Detecting composite image manipulation based on deep neural networks. In *International Conference on Systems, Signals and Image Processing*, pages 1–5. IEEE, 2017.

[18] D. Cozzolino, G. Poggi, and L. Verdoliva. Efficient dense-field copy–move forgery detection. *IEEE Transactions on Information Forensics and Security*, 10(11):2284–2297, 2015.

[19] D. Cozzolino, G. Poggi, and L. Verdoliva. Splicebuster: A new blind image splicing detector. In *IEEE International Workshop on Information Forensics and Security*, pages 1–6. IEEE, 2015.

[20] D. Cozzolino and L. Verdoliva. Noiseprint: a CNN-based camera model fingerprint. *arXiv preprint arXiv:1808.08396*, 2018.

[21] Y. Fan, P. Carré, and C. Fernandez-Maloigne. Image splicing detection with local illumination estimation. In *IEEE International Conference on Image Processing*, pages 2940–2944. IEEE, 2015.

[22] P. Ferrara, T. Bianchi, A. De Rosa, and A. Piva. Image forgery localization via fine-grained analysis of cfa artifacts. *IEEE Transactions on Information Forensics and Security*, 7(5):1566–1577, 2012.

[23] L. A. Gatys, A. S. Ecker, and M. Bethge. Image style transfer using convolutional neural networks. In *IEEE Conference on Computer Vision and Pattern Recognition*, pages 2414–2423, 2016.

[24] T. Gloe and R. Böhme. The'dresden image database'for benchmarking digital image forensics. In *ACM Symposium on Applied Computing*, pages 1584–1590. ACM, 2010.

[25] J. G. Han, T. H. Park, Y. H. Moon, and I. K. Eom. Efficient markov feature extraction method for image splicing detection using maximization and threshold expansion. *Journal of Electronic Imaging*, 25(2):023031, 2016.

[26] K. He, X. Zhang, S. Ren, and J. Sun. Deep residual learning for image recognition. In *IEEE Conference on Computer Vision and Pattern Recognition*, pages 770–778, 2016.

[27] S. Heller, L. Rossetto, and H. Schuldt. The ps-battles dataset-an image collection for image manipulation detection. *arXiv preprint arXiv:1804.04866*, 2018.

[28] M. Huh, A. Liu, A. Owens, and A. A. Efros. Fighting fake news: Image splice detection via learned self-consistency. In *The European Conference on Computer Vision*, September 2018.

[29] N. Krawetz and H. F. Solutions. A pictures worth... *Hacker Factor Solutions*, 6, 2007.

[30] C. Li, Q. Ma, L. Xiao, M. Li, and A. Zhang. Image splicing detection based on markov features in qdct domain. *Neurocomputing*, 228:29–36, 2017.

[31] G. Liu, F. A. Reda, K. J. Shih, T.-C. Wang, A. Tao, and B. Catanzaro. Image inpainting for irregular holes using partial convolutions. In *The European Conference on Computer Vision*, September 2018.

[32] Y. Liu, Q. Guan, X. Zhao, and Y. Cao. Image forgery localization based on multi-scale convolutional neural networks. In *ACM Workshop on Information Hiding and Multimedia Security*, pages 85–90. ACM, 2018.

[33] S. Lyu, X. Pan, and X. Zhang. Exposing region splicing forgeries with blind local noise estimation. *International Journal of Computer Vision*, 110(2):202–221, 2014.

[34] B. Mahdian and S. Saic. Using noise inconsistencies for blind image forensics. *Image and Vision Computing*, 27(10):1497–1503, 2009.

[35] O. Mayer and M. C. Stamm. Learned forensic source similarity for unknown camera models. In *IEEE International Conference on Acoustics, Speech and Signal Processing*, 2018.

[36] Y. Nirkin, I. Masi, A. T. Tran, T. Hassner, and G. Medioni. On face segmentation, face swapping, and face perception. In *IEEE Conference on Automatic Face and Gesture Recognition*, 2018.

[37] Y. Rao and J. Ni. A deep learning approach to detection of splicing and copy-move forgeries in images. In *IEEE International Workshop on Information Forensics and Security*, pages 1–6. IEEE, 2016.

[38] P. Rota, E. Sangineto, V. Conotter, and C. Pramerdorfer. Bad teacher or unruly student: Can deep learning say something in image forensics analysis? In *IEEE International Conference on Pattern Recognition*, pages 2503–2508. IEEE, 2016.

[39] R. Salloum, Y. Ren, and C.-C. J. Kuo. Image splicing localization using a multi-task fully convolutional network (mfcn). *Journal of Visual Communication and Image Representation*, 51:201–209, 2018.

[40] K. Simonyan and A. Zisserman. Very deep convolutional networks for large-scale image recognition. *arXiv preprint arXiv:1409.1556*, 2014.

[41] A. M. Stern, A. Casadevall, R. G. Steen, and F. C. Fang. Financial costs and personal consequences of research misconduct resulting in retracted publications. *Elife*, 3:e02956, 2014.

[42] J.-Y. Sun, S.-W. Kim, S.-W. Lee, and S.-J. Ko. A novel contrast enhancement forensics based on convolutional neural networks. *Signal Processing: Image Communication*, 63:149–160, 2018.

[43] B. Wen, Y. Zhu, R. Subramanian, T.-T. Ng, X. Shen, and S. Winkler. Coverage a novel database for copy-move forgery detection. In *IEEE International Conference on Image processing*, pages 161–165, 2016.

[44] Y. Wu, W. Abd-Almageed, and P. Natarajan. Deep matching and validation network: An end-to-end solution to constrained image splicing localization and detection. In *ACM on Multimedia Conference*, pages 1480–1502. ACM, 2017.

[45] Y. Wu, W. Abd-Almageed, and P. Natarajan. Busternet: Detecting copy-move image forgery with source/target localization. In *The European Conference on Computer Vision*, September 2018.

[46] Y. Wu, W. Abd-Almageed, and P. Natarajan. Image copy-move forgery detection via an end-to-end deep neural network. In *IEEE Winter Conference on Applications of Computer Vision*, pages 1907–1915. IEEE, 2018.

[47] Y. Wu and P. Natarajan. Self-organized text detection with minimal post-processing via border learning. In *IEEE International Conference on Computer Vision*, pages 5000–5009, 2017.

[48] S. Xingjian, Z. Chen, H. Wang, D.-Y. Yeung, W.-K. Wong, and W.-c. Woo. Convolutional lstm network: A machine learning approach for precipitation nowcasting. In *Advances in neural information processing systems*, pages 802–810, 2015.

[49] Q. Yang, F. Peng, J.-T. Li, and M. Long. Image tamper detection based on noise estimation and lacunarity texture. *Multimedia Tools and Applications*, 75(17):10201–10211, 2016.

[50] S. Zagoruyko and N. Komodakis. Wide residual networks. In E. R. H. Richard C. Wilson and W. A. P. Smith, editors, *British Machine Vision Conference*, pages 87.1–87.12. BMVA Press, September 2016.

[51] M. Zampoglou, S. Papadopoulos, and Y. Kompatsiaris. Large-scale evaluation of splicing localization algorithms for web images. *Multimedia Tools and Applications*, 76(4):4801–4834, 2017.

[52] K. Zhang, W. Zuo, Y. Chen, D. Meng, and L. Zhang. Beyond a gaussian denoiser: Residual learning of deep cnn for image denoising. *IEEE Transactions on Image Processing*, 26(7):3142–3155, 2017.

[53] Z. Zhang, Y. Zhang, Z. Zhou, and J. Luo. Boundary-based image forgery detection by fast shallow cnn. *arXiv preprint arXiv:1801.06732*, 2018.

[54] P. Zhou, X. Han, V. I. Morariu, and L. S. Davis. Two-stream neural networks for tampered face detection. In *IEEE Conference on Computer Vision and Pattern Recognition Workshops*, pages 1831–1839, 2017.

[55] P. Zhou, X. Han, V. I. Morariu, and L. S. Davis. Learning rich features for image manipulation detection. In *IEEE Conference on Computer Vision and Pattern Recognition*, pages 1907–1915. IEEE, 2018.

[56] P. Zhou, X. Han, V. I. Morariu, and L. S. Davis. Learning rich features for image manipulation detection. In *IEEE Conference on Computer Vision and Pattern Recognition*, 2018.

[57] J.-Y. Zhu, T. Park, P. Isola, and A. A. Efros. Unpaired image-to-image translation using cycle-consistent adversarial networks. In *IEEE International Conference on Computer Vision*, 2017.

[58] X. Zhu, Y. Qian, X. Zhao, B. Sun, and Y. Sun. A deep learning approach to patch-based image inpainting forensics. *Signal Processing: Image Communication*, 2018.